geosciences

MDPI

Article

What Pulsating H_2 Emissions Suggest about the H_2 Resource in the Sao Francisco Basin of Brazil

Lawrence Cathles [1,*] and Alain Prinzhofer [2]

[1] Department of Earth and Atmospheric Sciences, Cornell University, Ithaca, NY 14853, USA
[2] Geo4U Geosciences Integrated Services LTDA (Geo4U), Praia de Botafogo, 501–Botafogo, Rio de Janeiro, RJ–CEP 22250-040, Brazil; prinzhofer2@gmail.com
* Correspondence: lmc19@cornell.edu

Received: 12 February 2020; Accepted: 10 April 2020; Published: 17 April 2020

Abstract: Proterozoic sedimentary basins very often emit natural hydrogen gas that may be a valuable part of a non-carbon energy infrastructure. Vents in the Sao Francisco Basin in Brazil release hydrogen to the atmosphere mainly during the daylight half of the day. Daily temperature and the regular daily tidal atmospheric pressure variations have been suggested as possible causes of the pulsing of H_2 venting. Here, we analyze a ~550 m-diameter depression that is barren of vegetation and venting hydrogen mainly at its periphery. We show that daily temperature changes propagated only ~1/2 m into the subsurface and are thus too shallow to explain the H_2 variations measured at 1-m depth. Pressure changes could propagate deeply enough, and at the depth at which the cyclic variations are measured hydrogen concentration will have the observed phase relationship to atmospheric pressure changes provided: (1) the pressure wave is terminated by geologic barriers at about 25% of its full potential penetration distance, and (2) the volume of gas in the vents is very small compared to the volume of gas tapped by the venting. These constraints suggest that there is a shallow gas reservoir above the water table under the ~550 m-diameter barren-of-vegetation depression. The 1D-analytical and finite-element calculations presented in this paper help define the hydrogen system and suggest the further steps needed to characterize its volume, hydrogen flux and resource potential.

Keywords: hydrogen economy; natural hydrogen vents; Sao Francisco Basin; pulsing gas emission; atmospheric pressure tides

1. Introduction

Hydrogen gas may become an important part of the zero-carbon energy economy because its combustion produces only water vapor and no CO_2. Hydrogen is generally considered a vector of energy because it is an agent of energy transfer that needs to be manufactured from some other material, such as hydrocarbons or water, and thus carries energy from other sources. Several studies have shown, however, that there are natural sources of hydrogen that could be an important resource (Ward, 1933 [1]; Goebel et al., 1984 [2]; Newell et al., 2007 [3]; Sherwood-Lollar et al., 2014 [4]; Prinzhofer and Deville, 2015 [5]; Guélard et al., 2017 [6]; Prinzhofer et al., 2018 [7]). The Earth is naturally expelling native hydrogen through still-poorly determined physico-chemical processes.

As at the start of the petroleum era, we currently know only that hydrogen is seeping out of rocks and soils in many locations. Studies so far have focused on the chemistry of the seeps that have been discovered worldwide (Larin et al., 2014 [8]; Zgonnik et al., 2015 [9]; Deville and Prinzhofer, 2016 [10]; Prinzhofer et al., 2019 [11]) and the origin of the hydrogen (Larin, 1993 [12]; Gilevska, T., 2007 [13]; Milesi et al., 2015 [14]; Vacquand et al., 2018 [15]; Truche et al., 2018 [16]). The many seeps that have been found indicate the operation of an active hydrogen system, and transient

accumulations of hydrogen at relatively shallow depth are known (Mali, Prinzhofer et al., 2018 [7], USA, Goebel et al., 1984 [2]; Newell et al., 2007 [3]; Guélard et al., 2017 [5]). But we know little about the scale and economic potential of the hydrogen systems that are involved.

The most important parameter for gauging the magnitude of the hydrogen resource is the magnitude of the hydrogen (H_2) emission because it immediately suggests the probability of hydrogen accumulation under subsurface structures, and also indicates the sustainability of this source of energy. To better constrain the magnitude of the hydrogen emission, a permanent monitoring station has been installed at 16 °S in the dry, hot Sao Francisco Basin of Brazil. Venting is being monitored there with sensors that measure H_2 concentrations at ~1 m depth around the perimeter of a 550 m diameter vent (Prinzhofer et al., 2019) [11]. The data indicate daily pulses of hydrogen emission. The maximum concentration of H_2 in the venting gases usually occurs in the middle of the day, although some sensors have hydrogen concentration peaks at the beginning of the day, or even during the night. It appears that these variations are linked to complex external parameters such as biologic activity in the soils, temperature, atmospheric pressure, Earth tides, etc.

Importantly, the correlation between H_2 concentrations and atmospheric pressure is not linear, but presents a kind of hysteresis in which there is a delay between the pressure variation in free air, the hydrogen concentration measured by the sensors at 1 m depth, and the gas movements induced in the porous soil. The soil generally has very low water saturation above the water table several meters below the surface. This paper investigates whether the variation of hydrogen concentrations in soils could be caused by diurnal/nocturnal variations in temperature or atmospheric pressure.

H_2 gas is venting in the Sao Francisco Basin from slight topographic depressions that are circular, barren of vegetation, and aligned along a major fault. The water table is at 3 to 5 meters depth. The hydrogen venting from the 600 × 500 m study area is not continuous, but pulses on a daily cycle wherein H_2 is detected by shallow (1 m depth) sensors for only about half the day, usually centered on high noon. Prinzhofer et al. (2019) [11] have estimated the emission rate is between 7000 and 178,000 m^3 H_2 per day, based on the venting at Sensor 9 (Figure 1) where the volume of H_2 venting is greatest and the concentration of H_2 in the venting gas is sometimes above 1000 ppm. Hydrogen is thought to be generated in basins from the reduction of water attending ferrous to ferric iron oxidation (Welhan and Craig, 1979 [17]; Neal and Stranger, 1983 [18]; Abrajano et al., 1990 [19]; Sano et al., 1993 [20]; Charlou et al., 2002 [21]) and/or NH_4^+ decomposition at depths where the temperature exceeds 200 to 250 °C (Guélard et al., 2018) [22]. The H_2 concentration was found to be 50% to 80% (with the rest N_2 and several percent CH_4) in a deep drill hole in the Sao Francisco basin, and measurements at other sites in the basin found a source H_2 concentration ranging from 50% to ~100%. This suggests that the undiluted hydrogen source at the vent we analyze has a hydrogen concentration of at least 50%.

We investigate whether, and under what circumstances, daily changes in either surface temperature or atmospheric pressure can cause gas flow to reverse (e.g., air to flow into the ground) for half the day and thus potentially explain why H_2 is detected for only half a day. The initial method of analysis is to compute, for both temperature and pressure changes, the change in gas density as a function of depth, the variations in the rate of gas flow produced by these density changes, and the conditions under which the density-change-driven-flow could cause the flow of H_2-free air into the vent subsurface for about half the day. It is found that variations in atmospheric pressure could account for the diurnal variations in H_2 detection, but temperature variations cannot. The pressure-driven changes in hydrogen concentration at 1 m depth are then investigated quantitatively by comparing the timing and magnitude (phase relations between) of the calculated and observed modulation in hydrogen concentration. It is found that pressure variations must be blocked by a barrier of some kind when they have propagated about 25% of the distance they could potentially propagate into a gas-filled reservoir, and that the gas volume of the reservoir tapped needs to be at least 1000 times greater than the gas volume in the vent. These insights, obtained by simple 1D analytical and finite element analyses, suggest how the Sao Francisco hydrogen system is operating, how the system could be tested by future drilling, and the kind of future 3D modeling that will be required to define the operation of this hydrogen system.

2. Analysis

2.1. Site Characterisics

2.1.1. The Study Site

As illustrated in Figure 1, H_2 is venting from a 600 × 500 m depression that is barren of vegetation. One possibility is that the reduced conditions caused by hydrogen venting have killed the vegetation; another is that periodic flooding of the small depressions is he cause. To be neutral, we label the area A_{barren}. The study area is the large barren area shown in Figure 1 with A_{barren} = 300,000 m^2. It is venting hydrogen at an estimated rate of between 7000 and 178,000 m^3 H_2 per day (Prinzhofer et al., 2019) [11]. Assuming the concentration of the source is 50% H_2, the venting rate at depth, Q_{H2}, is between 14,000 and 356,000 m^3 per day. If the flow is uniform across the vent area, the gas flux is V_{deep} = Q_{H2}/A_{barren} = 0.05 to 1.2 m d^{-1}. The average concentration of H_2 in the discharge measured at ~1 m depth is ~100 ppm (Prinzhofer et al., 2019 their Figure 2) [11].

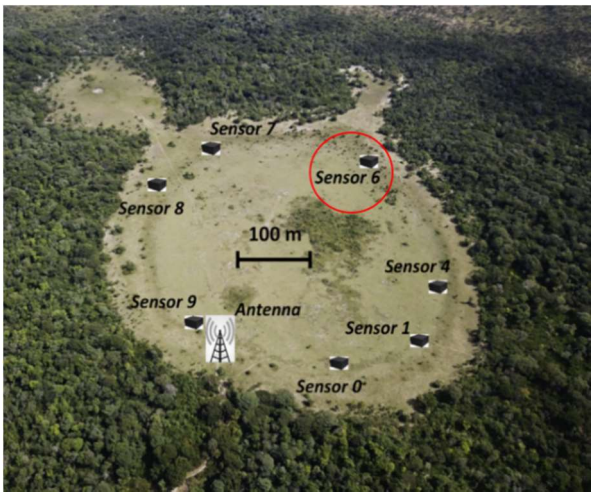


Figure 1. H_2 is venting in a pulsating fashion from the periphery of a 600 × 500 m topographical depression barren of vegetation in the Sao Francisco sedimentary basin of Brazil at latitude ~16 °S. Sensor 6 is circled in red. Figure is from Prinzhofer et al. (2019).

2.1.2. Daily Variations in T

The temperature ranges from 15 to 35 °C in the afternoons. Because the bare surface will likely be heated above the atmospheric temperature, the range of ground surface temperature will likely be greater than the average atmospheric temperature range.

2.1.3. Daily Variations in Atmospheric Pressure

The daily variations in atmospheric pressure are quite regular at the site and are available from a local meteorological station. Pressure peaks at about 10:00 local solar time, and the steepest part of the subsequent pressure decrease occurs at about 13:00 local solar time. The pressure change over the day is between 4 and 8 mbar. Figure 2A compares the atmospheric pressure variations on 14 August 2018 to the $[H_2]$ concentrations measured at 1 m depth by Sensor 6 on the same day. Peak $[H_2]_{sensor\text{-}6}$ occurs at ~13:00, coinciding with the maximum in the rate of atmospheric pressure decline.

Figure 2B separates out the diurnal and semidiurnal sinusoidal components of the atmospheric pressure change amplitudes of 1.5 and 1.2 mb and phase lags of 16 and 14 h, respectively. When summed these components replicate the observed pressure variations very closely (compare yellow and blue curves in Figure 2A).

Figure 2C shows the phase relationships between atmospheric pressure and the hydrogen concentration measured at Sensor 6. As in Figure 2A, hydrogen is detected when the atmospheric pressure is decreasing, but the figure shows a clear hysteresis between pressure change and the

hydrogen measurements that is diagnostic of pressure wave transmission into the subsurface. By hysteresis we mean that hydrogen concentrations measured in Sensor 6 when the atmospheric pressure is increasing are different from those measured when the atmospheric pressure is decreasing. In this case the contrast is dramatic since the hydrogen concentration is zero when pressure is increasing and positive when it is decreasing. The red circle in Figure 2C emphasizes that the maximum *[H₂]* is measured at 13:00 when the surface pressure is decreasing at its maximum rate (Figure 2A).

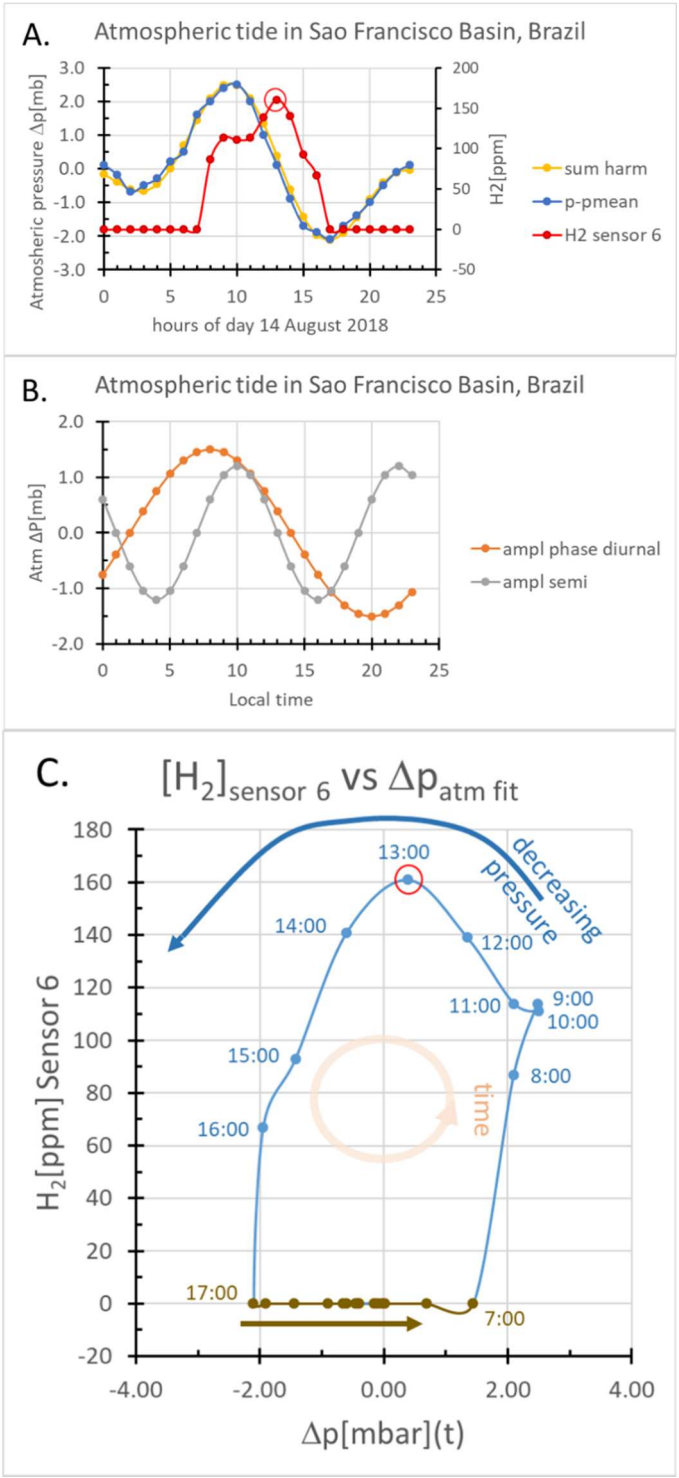


Figure 2. (**A**) Observed atmospheric pressure changes at Sao Francisco Basin H_2 vent, and the [H_2] concentrations measured at Sensor 6. (**B**) The pressure variations can be decomposed into diurnal and s semi-diurnal sinusoidal components which sum to accurately represent the observed variations

(yellow curve in A). (**C**) Phase relations between atmospheric pressure and [H_2] measured at Sensor 6.

The regular variations in atmospheric pressure are caused by atmospheric tides. At low latitudes, away from the much larger pressure variations associated with shifts of the polar front jets, the atmospheric tidal variations in pressure are typically mainly semi-diurnal with amplitudes of ~1.6 mb (Le Blancq, 2011 [23]). At our site the tidal atmospheric changes (2 mb amplitude) are similar in magnitude but have a strong diurnal component. We do not know why the daily atmospheric pressure variation at our site are more strongly diurnal than the norm.

2.2. Theoretical Analysis

This paper analyzes the hydrogen venting in the Sao Francisco basin analytically. This reveals the fundamental controls on the pulsing venting, but numerical simulations will ultimately be needed to gain a full understanding of the system. Our analysis is thus preliminary and preparatory. All symbols are defined in Table 1. Parameter values for the problem at hand are also given in the table, along with the method of their calculation or references for the values selected. Relationships given in the table indicate important physical dependencies. We consider both temperature and pressure wave transmission into the subsurface but concentrate on pressure transmission because we find that daily temperature changes penetrate only a few 10 s of centimeters and therefore cannot modulate hydrogen concentrations to a depth of one meter. Our method is to calculate the change in gas volume from either thermal expansion or compression and integrate this volume change to determine vertical (1D) gas velocity.

2.2.1. Thermal and Pressure Wave Propagation into the Subsurface

Surface temperature and pressure changes diffuse into the subsurface at rates and depths controlled by the subsurface thermal and hydraulic diffusivity, respectively. The diffusion equations both combine the heat and pressure flux equations with conservation of heat and mass and are identical in form and most clearly described in parallel. These equations describe how cyclic variations of temperature and pressure propagate from the surface at z = 0 into the subsurface (z negative):

The flux of heat described by Fourier's law and the flux of gas by Darcy's law are:

$$j = -K\frac{\partial T}{\partial z}\hat{z} \tag{1}$$

$$V = -\frac{k'}{\mu}\frac{\partial p'}{\partial z}\hat{z} \tag{2}$$

Conservation of mass requires:

$$\rho_T c_T \frac{\partial T}{\partial t} = -\nabla \bullet j = K_T \frac{\partial^2 T}{\partial z^2} \tag{3}$$

$$\frac{\partial T}{\partial t} = \kappa_T \frac{\partial^2 T}{\partial z^2}$$

$$\kappa_T = \frac{K_T}{\rho_T c_T}$$

$$\left(\beta_m + \phi\beta_f\right)\frac{\partial p'}{\partial t} = -\nabla \bullet V = \frac{k'}{\mu_{air}}\frac{\partial^2 p'}{\partial z^2} \tag{4}$$

$$\frac{\partial p'}{\partial t} = \kappa_p \frac{\partial^2 p'}{\partial z^2}$$

$$\kappa_p = \frac{k'}{\mu_{air}\left(\beta_m + \phi\beta_{air}\right)} \cong \frac{k'}{\mu_{air}\phi\beta_{air}}$$

In (4) we have used the fact that the compressibility of air is much greater than the compressibility of the soil matrix.

The final temperature (3) and pressure (4) diffusion equations differ only in their diffusivity parameters κ. We seek the subsurface solution for T(z,t) and p′(z,t) for z = 0 to −∞. Let α represent either T or p' and α_o the amplitude variation imposed at the surface. Defining $\bar{t} = t / P$, where P is the period of the harmonic variation imposed at the surface, the solution to Equations 3 and 4, (Carslaw and Jager, 1959. p65 [24]) is:

$$\alpha(z,\bar{t}) = \alpha_o e^{z/\delta} \cos\left(2\pi\bar{t} + z/\delta\right) \tag{5}$$

Where

$$\delta_\alpha = \sqrt{\frac{\kappa_\alpha P}{\pi}} \tag{6}$$

Because we want the rate of venting, we take the time derivative of (5):

$$\frac{\partial\alpha}{\partial t} = \frac{1}{P}\frac{\partial\alpha}{\partial\bar{t}} = -\frac{2\pi}{P}\alpha_o e^{z/\delta_\alpha} \sin\left(2\pi\bar{t} + z/\delta_\alpha\right) \tag{7}$$

Defining $\bar{z} = z/\delta_\alpha$, we can integrate (5) from some depth $\bar{z}_b$ to the surface (or sensor depth) to obtain the total rate of volume change from great depth to the subsurface (or up to sensor depth). By conservation of mass this must equal the gas flux, $V_{z=0}(t)$, out the top surface (or past the sensors). The sign depends on whether the forcing is by pressure or temperature change. The gas fluxes are:

$$V^{p'}_{\bar{z}=0}(t) = -\frac{2\pi}{P}\alpha_{p'o}\phi\beta_{p'}\delta_{p'}\int_{\bar{z}'=\bar{z}_b}^{0} e^{\bar{z}'} \sin\left(2\pi\bar{t} + \bar{z}'\right)d\bar{z}' \tag{8}$$

$$V^{T}_{\bar{z}=0}(t) = \frac{2\pi}{P}\alpha_{To}\phi\beta_T\delta_T\int_{\bar{z}'=\bar{z}_b}^{0} e^{\bar{z}'} \sin\left(2\pi\bar{t} + \bar{z}'\right)d\bar{z}' \tag{9}$$

Here α_o has been replaced by $\alpha_{p'o}$ or α_{To}, and the sign is such that there is volume expansion if the change in pressure is negative or the change in temperature is positive. Note the prime on $\bar{z}$ simply indicates that it is an integration variable.

If the depth of integration, $\bar{z}_b$, is sufficiently large that the underlying pressure or temperature variations are negligible, for example $\bar{z}_b$ = −10, the normalized integral, $\int_{\bar{z}=-10}^{0} e^{\bar{z}} \sin\left(2\pi\bar{t} + \bar{z}'\right)d\bar{z}'$ varies from −0.709 to +0.709 as $\bar{t}$ varies over its sinusoidal cycle. The phase shift between the temperature or pressure forcing applied at the surface ($\bar{z}$ = 0) and the venting flux V are both maximum for this deep integration. If $\bar{z}_b$ is shallow and the full subsurface thermal or pressure wave is not captured in the integration, the phase shift between the pressure or temperature and the venting flux V at the $\bar{z}$ = 0 is less and the rate of venting is less.

The maximum and minimum values of the harmonic gas flux at the surface are:

$$V_\alpha^{\max/\min}\left(z=0\right) = \pm\frac{(0.709)2\pi}{P}\alpha_o\phi\beta_\alpha\delta_\alpha \tag{10}$$

Since the gas flux is linear, we can add the deep H_2-bearing gas flux, V_{deep}, to (6) to obtain the total gas flux, $V^{total}_{z=0}(t)$:

$$V^{total}_{z=0}(t) = V_{deep} - \frac{2\pi}{P}\alpha_o\phi\beta_\alpha\delta\int_{\bar{z}'=-10}^{\bar{z}} e^{\bar{z}'} \sin\left(2\pi\bar{t} + \bar{z}'\right)d\bar{z}' \tag{11}$$

The H_2 emissions could be pulsating if:

$$V_{deep} < \frac{2\pi}{P}\alpha_o\phi\beta_\alpha\delta_\alpha(0.709) \tag{12}$$

If condition (12) is satisfied, the T-driven or p′-driven flow into the ground will exceed the base leakage rate of deep H_2-bearing gas (V_{deep}), H_2-free air could periodically surround the sensors, and

the sensors could then detect low H_2 concentrations. Since V_{deep} = 0.05 to 1.2 m^3 m^{-2} d^{-1}, the question is whether the right hand side of (12) can exceed this value.

- *The box model*

It is instructive to consider a simple (but unrealistic) "box" model where, as atmospheric pressure changes, gas pressure changes instantly and uniformly within the entire box. If the subsurface where hydrogen is venting is permeable enough to some depth b_{box}, the atmospheric pressure change can be transmitted immediately, and the venting flux will be coincident with the rate of atmospheric pressure change:

$$V_{box}(\bar{z}=0) = -\phi b_{box}\frac{\partial p}{\partial t}\beta_{p'} \tag{13}$$

For φ = 0.2, b_{box} = 1000 m, $\beta_{p'}$ = 10^{-5} Pa^{-1}, and $-\frac{\partial p}{\partial t}$ = 25 mb d^{-1} = 2500 Pa d^{-1}, the gas flux from the box V_{box} = 5 m d^{-1}. For later discussion it is important to emphasize that the assumption of very rapid pressure transmission means that there is no phase shift between surface pressure change and surface gas flux.

- *Advection-diffusion equation for [H2]*

It will take some time for gas moving into the subsurface to reach the sensors at 1 m depth, and on the way, there will be mixing with the gas in the subsurface. The advection–diffusion equation describes these phenomena. The 1D flux, j_{H2}, of H_2 (expressed as the volume fraction of H_2 in air) by diffusion and advection is:

$$j_{H2} = -D_E\frac{\partial[H_2]}{\partial z} + V_{air}[H_2] \tag{14}$$

where $[H_2]$ is the volume fraction of H_2 in air. By mass conservation:

$$\frac{\partial\varphi[H_2]}{\partial t} = -\nabla\bullet j_{H2} = \frac{\partial}{\partial z}D_E\frac{\partial[H_2]}{\partial z} - V_{air}\frac{\partial[H_2]}{\partial z} \tag{15}$$

where D_E is the effective diffusion constant of H_2 in the vent, and V_{air} is the vertical flux of air (m^3 of air passing through a plan area or 1 m^2 per second) in the portion of the vent considered (in this case the uppermost part). The effective diffusion constant $D_E = \frac{D\phi}{\tau}$, where D is the diffusion constant of H_2 in air, φ is the porosity of the vent sediments, and τ is the tortuosity of the pores in the sediments, which we take to equal 2. If we make *t, z and* $[H_2]$ non-dimensional by defining:

$$\begin{aligned} t &= \bar{t}\frac{b^2\varphi}{D_E} = \bar{t}\,\tau_D \\ z &= \bar{z}b \\ [H_2] &= [\bar{H}_2][H_2]_{deep} \\ N_{pe} &= \frac{Vb}{D_E} \end{aligned} \tag{16}$$

Equation (15) becomes:

$$\frac{\partial[\bar{H}_2]}{\partial\bar{t}} = \frac{\partial^2[\bar{H}_2]}{\partial\bar{z}^2} - N_{pe}\frac{\partial[\bar{H}_2]}{\partial\bar{z}} \tag{17}$$

where N_{pe} is the Peclet number (ratio of advection to diffusion).

Table 1. Parameter values in equations derived above.

Param.	Units	Definition	Value	Method/Comment
$_{oT}$	K	Amplitude harmonic $T_{z=0}(t)$	30	Ground changes > atmospheric.
$_{op'}$	Pa	Diurnal amplitude $p'_{z=0}(t)$ (lag 16h) Semidiurnal $p'_{z=0}(t)$ (14h phase lag)	150 120	Atmospheric tide has two harmonic components (Figure 2).
$_{T}$	-	Thermal expansion of air	3.3×10^{-3}	=1/T[K] = 1/298 for 25 °C.
$_{p'}$	-	Volumetric compression of ideal gas		=1/p = $1/10^5$ at atm. Pressure.
b	m	Depth of system Equation (17)	m	[H_2] changes only near the surface.
b_{box}	m	Depth extent box model Equation (13)	m	Large b_{box} needed for sufficient V_{air}
c_s	J kg^{-1} K^{-1}	Heat capacity of solid matrix	837	
c_{air}	J kg^{-1} K^{-1}	Heat capacity of water-saturated air	4380	
	m	Thermal skin depth	0.1: 0.107 0.2: 0.102 0.4: 0.098	$= \sqrt{\frac{\kappa_T P}{\pi}}, \quad P = 3600 \times 24\ s$ ·
$\delta_{p'}^{1d}$	m	Pressure skin depth for 1 day period	$_{p'}$ 0.1: 56.1 0.2: 39.7 0.4: 28.0	$= \sqrt{\frac{\kappa_{p'} P}{\pi}}, \quad P = 3600 \times 24\ s$ · Reduced by $\sqrt{2}$ for semidiurnal.
D	m^2 s^{-1}	Diffusion constant of H_2 in large excess of air	0.756×10^{-4} 6.45 m^2 d^{-1}	By comparison D_{CO2}= 0.208 x 10^{-4}. Values from web.
D_E	m^2 s^{-1}	Effective diffusion constant in vent	$_E$ 0.1: 0.323 0.2: 0.645 0.4: 1.29	$= \frac{D\phi}{\tau}$, values assume =2. Table units are m^2 per day.
	-	Porosity of vent subsurface	~0.4	
[H_2]	-	Volume fraction of H_2 in air		
$[H_2]_{1m}$	-	Volume fraction of H_2 in air at 1 m depth	<10^2–10^3 ppm	
$[H_2]_{deep}$	-	Fraction H_2 deep in the vent	0.5 to 1	Deep H_2 concentration ~1 from diverse observations (see text).
$[\overline{H}_2]$	-	H_2 as fraction of $[H_2]_{deep}$		=$[H_2]/[H_2]_{deep}$.
j	J m^{-2} s^{-1}	Heat flux	calculated	
k′	m^2	Permeability (10^{-12} m^2 = 1 Darcy)	10^{-12}	Near surface sandy soil is assumed to be very permeable.
K_T	W m^{-1} K^{-1}	Thermal conductivity of media	$_T$ 0.1: 0.843 0.2: 0.685 0.4: 0.498	Calculated at 25 °C with fabric theory mix of K_s and K_{air} with fabric mixing parameter = 0.3, see Luo et al. (1994) [25].
K_s	W m^{-1} K^{-1}	Matrix thermal conductivity	4	Sandy soil with some clay at 25 °C.
K_{air}	W m^{-1} K^{-1}	Air thermal conductivity	0.0261	Air at 25 °C. T Dependence weak.
$_T$	m^2 s^{-1}	Thermal dispersivity of media	$_T$ 0.1: 4.2×10^{-7} 0.2: 3.8×10^{-7} 0.4: 3.6×10^{-7}	$= \frac{K_T}{\rho_T c_T}$ ·
$_{p'}$	m^2 s^{-1}	Hydrodynamic dispersivity of H_2-filled media for 1 Darcy vent permeability	$_{p'}$ 0.1: 0.114 0.2: 0.057 0.4: 0.029	$\cong \frac{k'}{\mu_{H_2} \varphi \beta_{p'}}$, $_{p'}$ for air is half H_2.
N_{pe}	-	Peclet nbr (Equation 17)		$= \frac{Vb}{D_E} = \frac{(0.05)(100)}{0.648} = 7.72$
$_{air,}$ $_{H2}$	kg m^{-1} s^{-1}	dynamic viscosity of air	$_{air}$ =1.78×10^{-5} $_{H2}$ =8.74×10^{-6}	$_{air}$ = $_{air}$ $_{air}$.
$_{air}$	m^2 s^{-1}	kinematic viscosity of air	1.48×10^{-5}	Regression: $_{air}$ = $-1.1555(10^{-14})T^3 + 9.5728(10^{-11})T^2 + 3.7604(10^{-8})T - 3.4484(10^{-6})$, from WWW.
P	s	Period of P harmonic	24×3600	T surface change, tidal p′ change.
P	-	Period normalized to 1 day	1	P/(1 day).
p	Pa	Atmospheric pressure		
P′	kg m s^{-2}	Perturbation from atmos. pressure		
p'_o	kg m s^{-2}	Amplitude atm pressure change	200 to 400	Changes due to atmospheric tide.
$_T$	kg m^{-3}	Density of media	$_T$ 0.1: 2430	= $_s$(1-)+ $_{air}$.

			0.2 | 2160 0.4 | 1620	
ρ_s	kg m^{-3}	Density of solid matrix	2700	
ρ_{air}	kg m^{-3}	Density of air	1.1	Density of air at 25 °C.
C_{TCT}	J kg^{-1} K^{-1}	Volumetric heat capacity air-saturated soil	C_T *0.1* | 2×10^6 *0.2* | 1.8×10^6 *0.4* | 1.4×10^6	$= \rho_s C_s(1-\phi) + \rho_{air} C_{air}\phi$.
T	K	Temperature in degrees K	~298	
T_o	K or °C	Amplitude of imposed surface T(t)	>20	Can be greater if surface T>T_{air}.
	-	Tortuosity of sediment pores	2	
τ_D	d	Time normalization in Equation (16)		$= \frac{b^2\phi}{D_E}$.
V_{air}	m^3 m^{-2} d^{-1}	Flux of air containing H_2		$V_{air} = V_{cyclic} + V_{deep}$.
V_{cyclic}	m^3 m^{-2} d^{-1}	Flux of air driven only by changes p		
V_{deep}	m^3 m^{-2} d^{-1}	Deep (source) H_2 gas flux assuming 100% H_2 concentration	0.05 to 1.2	Estimated by Prinzhofer (2019) [11], assuming uniform venting in barren zone.
$V_{T^{max}}$	m d^{-1}	Maximum flux into subsurface from T(t)	$V_{T^{max}}$ 0.1 | 0.005 0.2 | 0.009 0.4 | 0.018	$= \frac{2\pi}{(P=1d)} \alpha_{oT} \varphi \beta_T \delta_T (0.709)$
$V_{p',max}$ diurnal	m d^{-1}	Maximum flux into subsurface from diurnal p′(t), $\alpha_{op'}$ =150 Pa. From equ. 6a. A 1 darcy subsurface permeability is assumed.	$V_{p',max}$ 0.1 | 0.037 0.2 | 0.053 0.4 | 0.075	$= \frac{2\pi}{(P=1d)} \alpha_{op'} \varphi \beta_{p'} \delta_{p'}^{1d} (0.709)$
$V_{p',max}$ Semi-diurnal	m d^{-1}	Maximum flux into subsurface from semidiurnal p′(t), $\alpha_{op'}$ = 120 Pa. From Equation 8. A 1 darcy vent permeability is assumed.	$V_{p',max}$ 0.1 | 0.042 0.2 | 0.060 0.4 | 0.084	$= \frac{2\pi}{(P=0.5d)} \alpha_{op'} \varphi \beta_{p'} \frac{\delta_{p'}^{1d}}{\sqrt{2}} (0.709)$

2.3. Site Analysis

2.3.1. The Minimum Criterion for $[H_2]_{Station\text{-}6}$ Modulation

Whether the pulsing H_2 leakage criterion (9) is met depends on the parameter values. The last 3 lines in the Table 1 show the calculated cyclic gas inflow rates for temperature and pressure variations at the Sao Fancisco site. The maximum temperature-driven gas influx is an order of magnitude less than the pressure-driven influx, and too small to reverse even Prinzhofer's lowest venting estimate. The pressure-driven influx, on the other hand, could reverse the $[H_2]$ venting if the venting were at the low end of Prinzhofer's estimated range. For convenience we show the comparison in Table 2.

Table 2. Deep H_2 flux estimated by Prinzhofer, assuming the concentration in the deep venting gas is 50% H_2 compared to air flux in and out of vent that is driven by tidal atmospheric pressure changes. The air flux exceeds the venting flux for venting fluxes at the low end of the range estimated by Prinzhofer for a subsurface permeability of 1 Darcy.

Estimation Method	H_2 or Air Flux
Prinzhofer V_{deep} for 50% H_2 concentration	0.05 to 1.2 $m^3\ m^{-2}\ d^{-1}$
Calculated p-driven influx for φ = 0.1 to 0.4	0.079 to 0.159 $m^3\ m^{-2}\ d^{-1}$
Calculated T-driven influx for φ = 0.1 to 0.4	0.005 to 0.018 $m^3\ m^{-2}\ d^{-1}$

The calculations assume a subsurface permeability of 1 Darcy, and porosities between 0.1 and 0.4. The two harmonic components of pressure-driven gas flow in Table 1 are summed to produce the values in the Table 2. The pressure-driven gas flux is not very sensitive to porosity (factor of 2 change for a factor of 4 change in porosity). This $\sqrt{\phi}$ dependence arises because $\delta_{p'}$ depends on $1/\sqrt{\phi}$ (see Table 1). For a subsurface permeability of 10 darcies, $\delta_{p'}^{1d}$ would be increased by $\sqrt{10} = 3.2$, and the calculated pressure-driven air flux into the ground would range between 0.25 and 0.5 $m^3\ m^{-2}\ d^{-1}$.

Diurnal temperature changes penetrate so little into the subsurface that they cannot affect H_2 a meter below the surface. From Table 1, the thermal skin depth for daily temperature variations is at most 10 cm. This means that at 20 cm depth the temperature variation will be 10% of that at the surface, and at 40 cm, 1%. Temperature variations thus do not appear to be a viable way to explain $[H_2]$ variations measured at 1 m depth in the Sao Francisco basin. We therefore do not consider them further in this paper.

2.3.2. Pressure-driven Subsurface Gas Fluxes

Figure 3 shows the changes in pressure, the negative of the rate of pressure change (a proxy for decompression since gas expansion occurs when the pressure decreases), and the gas venting rate, all as a function of depth in meters into the subsurface. The calculated pressure changes take into account the resistance to gas venting offered by a 1-Darcy subsurface with 20% porosity. Note that at depth the pressure changes are out of phase with the surface pressure changes. The venting flux integrates the changes in gas volume from a depth where they are negligible to the surface. The profiles are integrated here from $\bar{z}$ = −10 to 0 (z = −394 m to 0) using Equation (14) with V_{deep} = 0, but the profiles are displayed in Figure 3 only to 120 m depth. The air flux profiles in the last panel are labeled "cyclic" to emphasize that they are produced by the cyclic daily changes in atmospheric tidal pressure only.

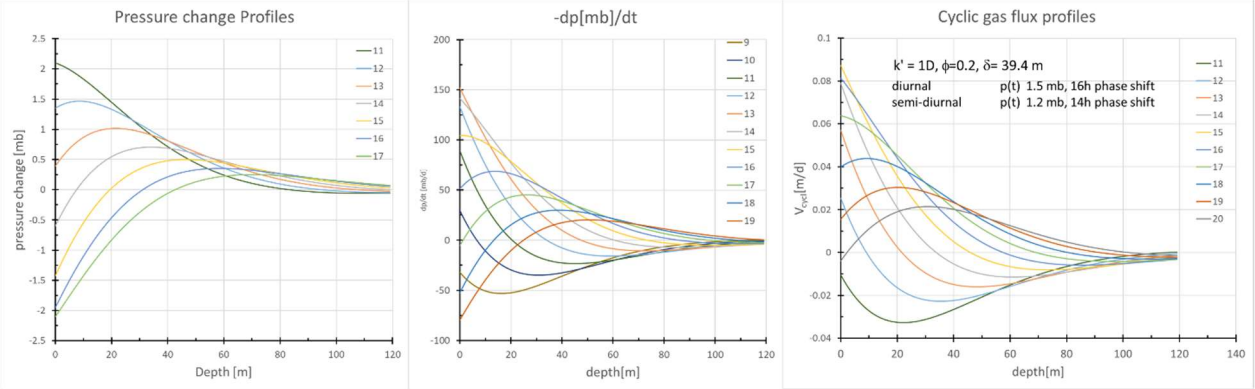


Figure 3. Calculated profiles of (**left**) pressure, (**middle**) the negative of the rate of pressure change (a proxy for gas decompression), and (**right**) the gas venting rate. Changes are caused by the changes atmospheric pressure shown in Figure 2. The subsurface permeability is 1 Darcy; the porosity 0.2 as shown in the legend in the last panel. The curves are for different hours of the day as indicated by the color key at the upper right of each diagram.

Figure 4A compares the calculated surface venting rate (black curve), the negative of the surface rate of pressure change (blue curve), and the H_2 concentration measured by Sensor 6 for 14 August 2018 (orange curve). The atmospheric pressure is decreasing at a maximum rate at 13:00 (blue curve peak). The maximum H_2 concentration measured by Sensor 6 (and most of the other sensors show in Figure 1) occurs at the same time (orange curve peak). On the other hand, the surface venting rate (black curve) peaks two hours later at 15:00.

Figure 4B shows the relationship between atmospheric pressure changes and the rate of surface gas efflux (V_{cyclic}). There is considerable hysteresis between the gas flux at 1.2 m depth and the surface pressure changes that produce this flux. The changes in gas flux values are not the same when the surface pressure is increasing as they are when it is decreasing. Figure 4C shows the relationship between the measured $[H_2]$ at Sensor 6 and the calculated cyclic gas flux at 1 m depth. Again, there is substantial hysteresis, and the hysteresis is very similar to that observed and shown in Figure 2C.

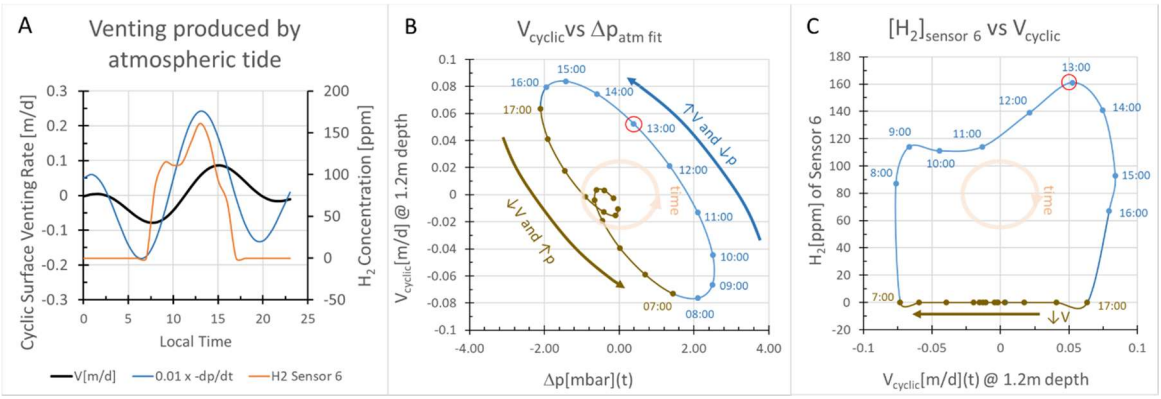


Figure 4. (**A**) The calculated gas venting rate at the surface (black curve) plotted versus local time for August 14, 2018. The blue curve shows the negative of the rate of change in atmospheric pressure at the surface. The orange curve shows the H_2 concentration measurements in Sensor 6 as a function of local time. The peaks in the H_2 concentration and –dp/dt coincide at 13:00, but the peak in surface venting rate is shifted by 2 h and occurs at 15:00. (**B**) The calculated gas flux V_{cyclic} at the surface is phase lagged relative to atmospheric pressure variations. (**C**) Calculated V_{cyclic} at 1.2 m depth is phase lagged relative to measured $[H_2]_{1m}$ at Sensor 6 is a fashion similar to atmospheric pressure variations shown in Figure 2C. The red circles indicate the time maximum $[H_2]_{1m}$ is observed in Sensor 6.

Figure 5 shows that if the cyclic (compression/decompression) gas flux comes from only the shallowest parts of the full system (the first 10 m of the curves shown in Figure 3), the phase shift with respect to the peak $[H_2]_{Sensor\text{-}6}$ is reduced. If the compression/decompression gas flux derives from

~10 m (= 0.25 $\delta_{p'}^{1d}$, where $\delta_{p'}^{1d}$ = 39.4 m) of the subsurface ($\bar{z}_b$ = 0.25 in Equation 9), the maximum in the surface venting rate (gray curve) nearly coincides in time with the maximum measured H_2 concentration. Note, however, that the magnitude of the gas flux is strongly reduced from the black curve (Figure 5A) where gas is expelled from all depths.

Figure 5B shows that the air flux profiles are nearly linear if they originate in only the upper 10 m of the profiles shown in Figure 3. Their linearity indicates that the upper part of the vent is behaving like the simple box model defined in Equation (16) where it is assumed that all the air in the subsurface is compressed equally and at the same time as the surface pressure changes. In the box case, the integrated flux will increase linearly from zero at $\bar{z}_b$, as is nearly the case in Figure 5B.

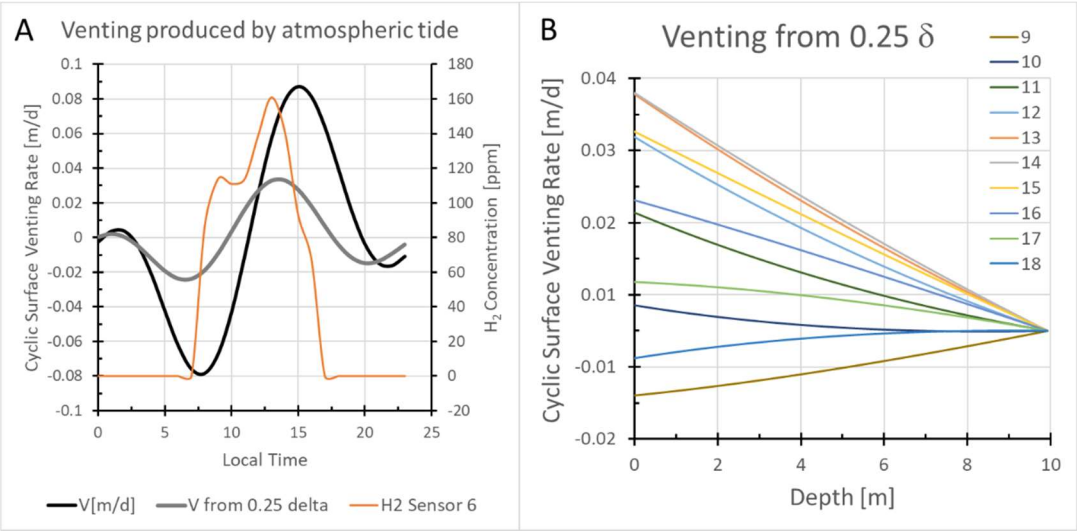


Figure 5. (**A**) The maximum cyclic gas flux calculated from a depth of 0.25δ (10 m depth for δ = 39.4 m) is more in phase with the maximum measured H_2. (**B**) Depth profiles of gas flux from 09:00 to 18:00. The depth profiles are almost linear and therefore approximate the flux profiles that would occur in a simple box model of the kind described in the box model section.

2.3.3. Box Model Advection/Diffusion Calculations of [H_2] at 1 m Depth

For a rise in atmospheric pressure to cause a drop in H_2 concentration at 1 m depth, air must penetrate at least that deep. This is a significant constraint: The air velocity v_{air} equals V_{air}/φ, so for φ = 0.2 and V_{air} = 0.05 m d^{-1} (the low flux estimate of Prinzhofer), the air velocity is 0.25 m d^{-1}. The atmospheric tide drives air into the ground for at most half a day, so the depth of air penetration for this low H_2 flux estimate is at most ~12 cm, which is much less than the depth of the sensors. To reach 1 m depth, the influx must be at least 8 times greater, e.g., V_{air}~0.4 m d^{-1}. Similarly, dilution of the effluent H_2 gases by influent air must be quite substantial for the measured $[H_2]_{1m}$ concentrations to be 100 to 1000 ppm. A simple stirred tank mixing model suggests reducing $[H_2]_{1m}$ by a factor of 1000 (from 50% H_2 to 500 ppm) would require mixing one volume of deep hydrogen-rich gas with ~7 volumes of air. Thus, from both these perspectives, the air influx must be about an order of magnitude greater than Prinzhofer's low estimate or ~0.05 m d^{-1}.

The advection–diffusion Equation (17) can be used to model the $[H_2]$ concentration at 1 m depth. The thickness of the "box" must be ~1000 m to produce cyclic air velocities large enough to dilute the hydrogen concentration at 1 m depth by the large amounts observed. This is an unrealistically large depth but suitable for our heuristic calculations here. The calculations start with the initial steady state $[H_2]$ profile in b_{box} for the assumed deep gas flux V_{deep}. This initial profile is then modified by the cyclic tidal air movements. The gas flux is constant but time varying at its 1-m-deep box value over the depth interval of analysis. The concentration changes produced by the cyclic variations in air flow are calculated to a much shallower depth, $b \ll b_{box}$, using Galerkin finite element methods (Baker and

Pepper, 1991 [26]) because the changes in $[H_2]$ induced by the cyclic air flux do not extend very far into the subsurface (< 25 m).

The calculations proceed in 1 h timesteps with 100 sub-timesteps. For plotting, $[H_2]$ is normalized by dividing by the deep H_2 concentration: $[\overline{H}_2] = [H_2]/[H_2]_{deep}$. The bottom boundary condition is Neuman wherein the H_2 flux equals $V_{deep}[\overline{H}_2]_{deep}$ and $[\overline{H}_2]_{deep} = 1$ (100% H_2). The top boundary is Dirichlet, $[\overline{H}_2]_{z=0} = 0$. Four daily pressure cycles are computed, and the last selected for plotting. b_{box} = 1000 m and V_{deep} = 0.1 m d^{-1}. There are 100 finite elements in the 25 m interval calculated. The surface air venting rate varies from -3.4 to + 5 m d^{-1}. Calculating for 200 instead of 100 finite elements in the interval from the surface to b = 25 m makes no difference to the results. The 200 element curves exactly overlie the 100 element blue curves, showing the 100 element calculation has more than enough depth resolution.

Figure 6 shows the changes in the $[\overline{H}_2]$ calculated as a function of depth and time of day for the atmospheric pressure variation of 14 August 2018 in the Sao Francisco Basin of Brazil. The insert in each panel shows the gas flux at the surface over the interval plotted. It can be seen that the tidal air flux produces dramatic changes in near surface hydrogen concentrations. Periods of air inflow drive the near-surface $[\overline{H}_2]_m$ concentration to lower values. Periods of air outflow increase the near-surface $[\overline{H}_2]_m$. The H_2 concentration varies between the surface and ~20 m depth. Below this depth the H_2 concentration is at the deep, up-flow value.

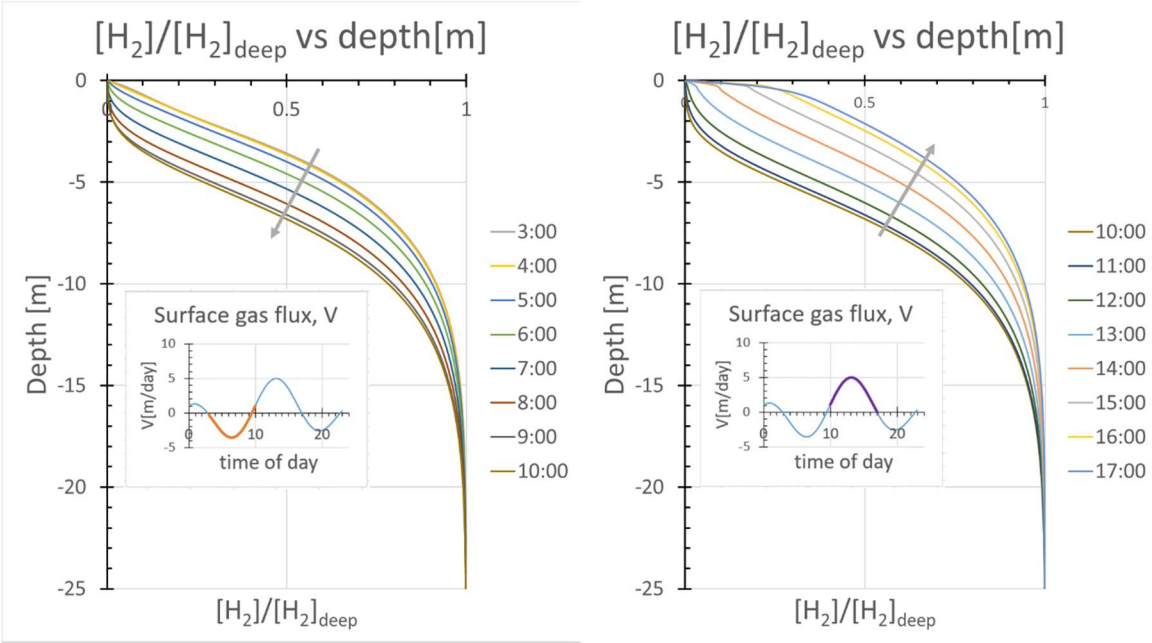


Figure 6. Calculated profiles of $[\overline{H}_2]$ for b_{box} = 1000 m and V_{deep} = 0.1 m d^{-1} for various times during 14 August 2018. The insert in each panel shows the calculated venting rate, highlighting the interval of the day when the profiles are plotted. The legend lists the time of day of each profile.

Figure 7 shows the calculated hydrogen concentration at 1 m depth, $[\overline{H}_2]_m$ on 14 August 2018. Periods of air inflow drive the near-surface H_2 concentration to very low values except for a small peak at ~3 AM. Periods of venting elevate the 1 m depth concentrations to 37% of the deep input concentration. The calculated variations in $[H_2]_m$ are offset from those observed (orange curve) by about ~3 h. The calculated modulation of $[\overline{H}_2]_m$ is strongly dependent on the vertical extent of the high permeability "box". The dashed blue line shows the comparatively small variation in $[\overline{H}_2]_m$ calculated for b_{box} = 200 m.

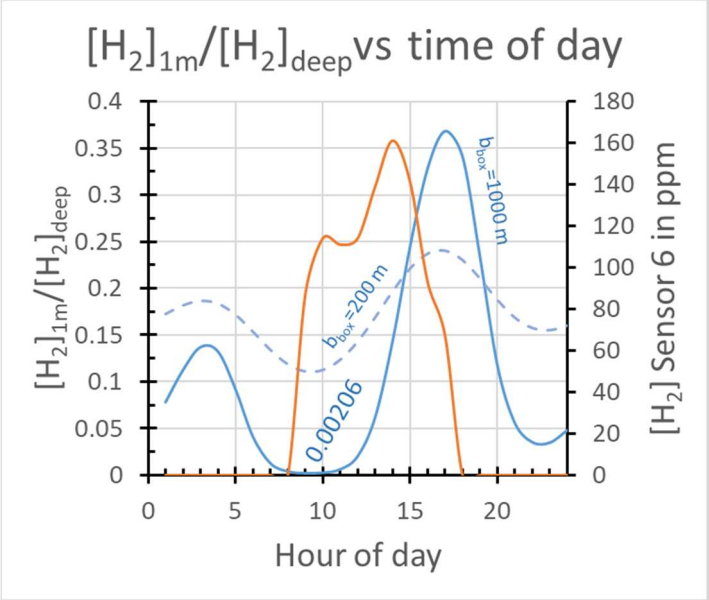


Figure 7. Computed $\left[\overline{H}_2\right]_{1m}$ for b_{box} = 1000 m and V_{deep} = 0.1 m d^{-1} (blue curve) is compared to the ppm $\left[H_2\right]_{1m}$ observed (orange curve). The dashed blue curve the H_2 profile computed for b_{box} = 200 m.

Finally, Figure 8 shows that, as expected, there is no substantial hysteresis between $\left[H_2\right]_{1m}$ and atmospheric pressure for the box model calculations. This is in strong contrast to observations (Figure 2C). Also, the calculated $\left[H_2\right]_{1m}$ concentration continues to increase until the gas efflux reverses (e.g., it is maximum at 17:00), rather than peaking when the rate of pressure change is greatest at 13:00 (red circle).

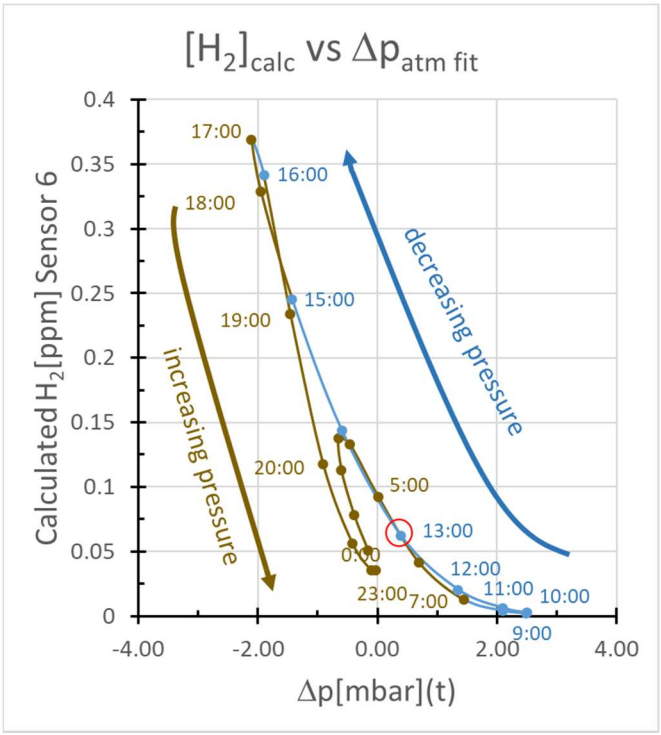


Figure 8. Phase relationship between $\left[H_2\right]_{1m}$ and the atmospheric pressure changes that drive the cyclic gas flow calculated in the box model. Unlike observations (Figure 2C), no substantial hysteresis is suggested by the box model calculations. The red circle marks the time maximum $\left[H_2\right]_{1m}$ is observed in Sensor 6.

3. Discussion

From the above analysis, it is clear that the atmospheric pressure tide could cause the pulsation in hydrogen concentration measured at 1 m depth. The main evidence supporting the hypothesis that atmospheric pressure changes are modulating the measured hydrogen concentration is the hysteresis in the observed Δp′ vs. $[H_2]_{1m}$ curve shown in Figure 2C. Figure 4C shows that the slow calculated diffusion of pressure into the subsurface produces a hysteresis between the rate of venting at 1.2 m depth, $V_{1.2m}$, and the measured $[H_2]_{1m}$ that is very similar in form to that observed between Δp′ and $[H_2]_{1m}$. (Note, the circulation is the same if $\Delta p'$ is replaced by $-\Delta p'$.) If $[H_2]_{1m}$ is proportional to $V_{1.2m}$, this hysteresis similarity strongly suggests the diffusion of pressure into the subsurface is the cause of the measured pulsing of the hydrogen venting.

A substantial reservoir of gas (compared to the volume of gas in the vents) must be compressed or expanded by the atmospheric pressure changes for hydrogen-free atmospheric air to be drawn to sensor depth. For the simple "box" model calculated above, the box must be ~1000 m thick to change $[H_2]_{1m}$ in a fashion similar to that observed (Figure 7). Instantaneous pressure transmission to 1000 m depth would require an unrealistically high subsurface permeability, so the box depth of 1000 m simply indicates that the reservoir gas volume affected by atmospheric pressure changes must be at least ~1000 times larger than the gas volume between the surface and the H_2 sensor at 1 m depth. Pressure wave calculations show that, in addition, the volume of gas accessible to the pressure wave must be about 25% of the full volume with which it could interact. This is required for the maximum venting rate, V, to coincide with the maximum $[H_2]_{1m}$ (Figure 5A). If the vent has a very low gas volume compared to the reservoir with which it interacts, there will be very little transit delay for incoming air to reach the H_2 gas sensors at 1 m depth. It is important to emphasize that the box modeling is 1D. Flow arises from vertical compression and decompression only. In reality gas would be supplied to vents laterally as well as vertically. Thus, the 25% of the potential draw should be interpreted as 25% of the 3D volume that feeds a particular vent.

It is reasonable that $[H_2]_{1m}$ should be maximum at the maximum venting rate at 1 m depth. The advection–diffusion solution shown in Figure 8 seems to suggest differently. It shows the maximum $[H_2]_{1m}$ occurs at the end of venting just before inflow begins. However, it is a 1D calculation that considers only vertical diffusion. In actuality, H_2 diffuses laterally from the vent, and, as gas rich in H_2 approaches the surface H_2 will diffuse laterally and be diluted. This dilution will be minimum when the gas efflux is maximum, and thus the maximum $[H_2]_{1m}$ should coincide with the maximum venting rate.

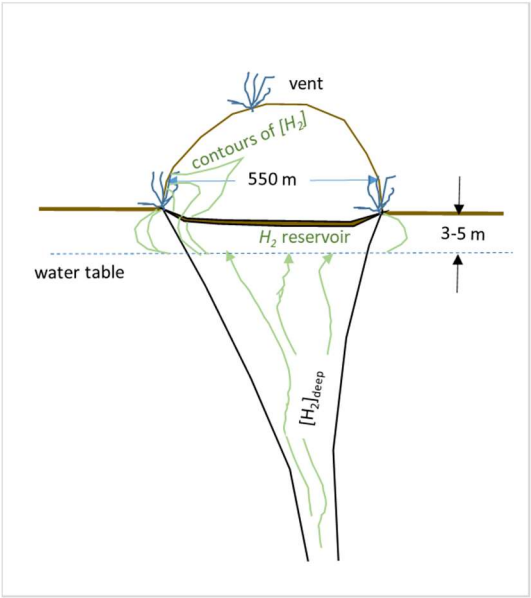


Figure 9. Schematic of H2 vent system suggested by the modeling results.

Observations as well as these modeling results suggest that hydrogen is venting from a shallow reservoir lying between the surface and the water table under the barren zone, and that the venting occurs mainly on the periphery, as shown in Figure 9. The barren zone is a small topographic depression that fills periodically with water. It is plausible that the top of the barren zone could be less permeable than its periphery because, due to periodic flooding, it receives more fine sediment deposition, has more evaporative salt deposition, and is more altered. Because slumping permeability might also be concentrated at the barren zone margins. If the upper layer of the central portion of the barren zone is relatively impermeable, but underlain by permeable sediments, a sealed H_2 reservoir could exist in the permeable sediments between the surface and the water table. The hypothetical reservoir could extend outside the barren zone if the sediments above the water table were as permeable outside as inside the barren zone. The reservoir in Figure 9 is shown being filled from depth by relatively pure (50 to 100%) hydrogen gas. Gas pushed into and out of the reservoir by atmospheric pressure tides through the periphery vents dilutes the reservoir near these vents as illustrated by the green hydrogen concentration contours surrounding the leftmost vent in Figure 9. Different perimeter vents will interact with the reservoir in slightly (and perhaps substantially) different ways if the permeability and porosity vary around the periphery of the reservoir. The time and concentration of the peak hydrogen concentration at different sensors could therefore differ as observed. The vents will operate as observed provided the three-to-five-meter-thick reservoir constitutes ~25% of the potential pressure wave penetration depth and the gas volume in the vents is a very small fraction of the volume compressed and decompressed by the atmospheric pressure tides impacting each vent.

The possibility that the vent system is operating as illustrated in Figure 9 can be tested in several ways: A gas probe in the center of the barren zone would test if there is a gas reservoir between a sealed surface and the water table. The hydrogen concentration in the center of the barren zone should be > 50% (or at least much greater than near the vents). Gas probes into the reservoir near sites of venting on the periphery could show how $[H_2]$ varies away from the vents. The gradient in $[H_2]$ and pressure variations at these probes could confirm the hypothesis that atmospheric-pressure variations cause the observed changes in measured H_2. Measurements of permeability and porosity would also test this hypothesis and would provide data for the kind of 3D finite element analysis that will be needed to accurately model the H_2 venting. Drill holes outside the barren zone would test the extent of the H_2 reservoir.

There is much that is not covered in our analysis. For example, as the water table at the base of our hypothetical H_2 reservoir rises and falls, accumulated H_2 will be expelled and diluted. Tracking these changes could be important to the H_2 content of the reservoir. The magnitude of H_2 venting is best provided, at least in the short term, by integrating the H_2 efflux from the periphery of the barren zone as has been done by Prinzhofer et al. (2019). We add nothing to Prinzhofer's estimates of the total H_2 venting rate in this paper. Rather, the analysis presented in this paper suggests the kind of system that could operate as observed. Ultimately 3D finite element modeling will be needed to define the hydrogen resource. For 3D modeling to contribute beyond the analysis offered here, however, more needs to be known about the shallow H_2 reservoir and its relation to the vents on the periphery of the barren zone. The needed information can be obtained by gas probe or shallow drilling.

4. Conclusions

This paper analyzes whether pressure- or temperature-driven air flow can explain the temporal variations in hydrogen concentration measured at 1 m depth along the perimeter of a 550 m diameter, largely barren depression in the Sao Francisco Basin in Brazil. Although the temporal variations could be caused by other processes such as solid earth tides or temperature-dependent bacterial H_2 generation, etc., we find:

1. The variations in hydrogen concentration measured at 1 m depth could be caused by propagation of a pressure wave into the subsurface, but not by the propagation of a thermal

wave. Diurnal temperature changes penetrate less than a meter into the subsurface and produce only weak perturbations of gas flow above the one-meter sensor depth.
2. The propagation of a pressure wave truncated at 25% of its potential penetration could produce changes in hydrogen concentration at 1 m with a phase shift relative to atmospheric tidal pressure changes similar to that most commonly observed.
3. To change *[H_2]* concentrations at 1 m depth, the gas volume in each vent needs to be < 1/1000th of the reservoir gas volume with which atmospheric pressure variations interact.
4. The venting system we infer here from observations and calculations is illustrated in Figure 9. The characteristics of this hypothetical system should be tested by measuring reservoir hydrogen concentrations with gas probes or by drilling as indicated in the discussion section.

Author Contributions: L.C. was responsible for the modeling, A.P. for field geology and framing the problem to be addressed. Both contributed equally to the writing of the paper. All authors have read and agreed to the published version of the manuscript.

Funding: The work reported here was not supported by any grant by any agency.

Acknowledgments: We thank the Scientific Direction of Engie S.A. for having launched the Natural H_2 Project. The sensors installed in Brazil that allowed monitoring measurements were developed by the Engie Laboratory CRIGEN. We specially thank Fabian Rupin for the last version of these sensors and Joao Françolin (Georisk) for his geological collaboration in the field and for data acquisition.

Conflicts of Interest: The authors declare no conflicts of interest.

References

1. Ward L.W. Inflammable gases occluded in the pre-Palaeozoic rocks of South Australia. *Trans. R. Soc. S. Aust.* **1933**, *57*, 42–47.
2. Goebel, E.D.; Coveney, R.M.J.; Angino, E.E.; Zeller, E.J.; Dreschhoff, G.A.M. Geology, composition, isotopes of naturally occurring H_2/N_2 rich gas from wells near Junction City, Kansas. Oil & Gas Journal **1984**, *82*, 215–222.
3. Newell, K.D.; Doveton, J.H.; Merriam, D.F.; Gilevska, T.; Waggoner, W.M.; Magnuson, L.M. H2-rich and Hydrocarbon Gas Recovered in a Deep Precambrian Well in Northeastern Kansas. *Nat. Resour. Res.* **2007**, *16*, 277–292.
4. Lollar, B.S.; Onstott, T.C.; Lacrampe-Couloume, G.; Ballentine, C.J. The contribution of the Precambrian continental lithosphere to global H2 production. *Nature* **2014**, *516*, 379–382.
5. Prinzhofer A.; Deville E. Hydrogène naturel. La prochaine révolution énergétique. Avaiable online: https://www.belin-editeur.com/hydrogene-naturel-la-prochaine-revolution-energetique (accessed on 16 April 2020)
6. Guélard, J.; Beaumont, V.; Rouchon, V.; Guyot, F.; Pillot, D.; Jézéquel, D.; Ader, M.; Newell, K.D.; Deville, E. Natural H2in Kansas: Deep or shallow origin?. *Geochem. Geophys. Geosystems* **2017**, *18*, 1841–1865.
7. Prinzhofer, A.; Cissé, C.S.T.; Diallo, A.B. Discovery of a large accumulation of natural hydrogen in Bourakebougou (Mali). *Int. J. Hydrogen Energy* **2018**, *43*, 19315–19326.
8. Larin, N.; Zgonnik, V.; Rodina, S.; Deville, E.; Prinzhofer, A. Larin V.N. Evidences for natural molecular hydrogen seepages associated with rounded subsident structures. Part 1: The craton of European Russia. *Nat. Resour. Res.* **2014**, *24*, 369–383. doi:10.1007/s11053-014-9257-5.
9. Zgonnik, V.; Beaumont, V.; Deville, E.; Larin, N.; Pillot, D.; Farrell, K.M. Evidence for natural molecular hydrogen seepage associated with Carolina bays (surficial, ovoid depressions on the Atlantic Coastal Plain, Province of the USA). *Prog. Earth Planet. Sci.* **2015**, *2*, 121.
10. Deville, E.; Prinzhofer, A. The origin of N2-H2-CH4-rich natural gas seepages in ophiolitic context: A major and noble gases study of fluid seepages in New Caledonia. *Chem. Geol.* **2016**, *440*, 139–147.
11. Prinzhofer, A.; Moretti, I.; Françolin, J.; Pacheco, C.; D'Agostino, A.; Werly, J.; Rupin, F. Natural hydrogen continuous emission from sedimentary basins: The example of a Brazilian H2-emitting structure. *Int. J. Hydrogen Energy* **2019**, *44*, 5676–5685.
12. Larin, N. *Hydridic Earth The New Geology of our Primortidally Hydrogen-rich Planet Translation;*.Polar Publishing: Maple Ridge, BC, Canada, 1993, pp. 247.

13. Gilevska, T.; Voglesonger, K.; Lin, L.-H.; Lacrampe-Couloume, G.; Telling, J.; Abrajano, T.; Onstott, T.; Pratt, L.M. Hydrogeologic Controls on Episodic H2 Release from Precambrian Fractured Rocks—Energy for Deep Subsurface Life on Earth and Mars. *Astrobiology* **2007**, *7*, 971–986. doi:10.1089/ast.2006.0096.
14. Milesi, V.P.; Guyot, F.; Brunet, F.; Richard, L.; Recham, N.; Benedetti, M.F.; Dairou, J.; Prinzhofer, A. Formation of CO2, H2 and condensed carbon from siderite dissolution in the 200–300°C range and at 50MPa. *Geochim. et Cosmochim. Acta* **2015**, *154*, 201–211.
15. Vacquand, C.; Deville, E.; Beaumont, V.; Guyot, F.; Sissmann, O.; Pillot, D.; Arcilla, C.; Prinzhofer, A. Reduced gas seepages in ophiolitic complexes: Evidences for multiple origins of the H2-CH4-N2 gas mixtures. *Geochim. et Cosmochim. Acta* **2018**, *223*, 437–461.
16. Truche, L.; Joubert, G.; Dargent, M.; Martz, P.; Cathelineau, M.; Rigaudier, T.; Quirt, D. Clay minerals trap hydrogen in the Earth's crust: Evidence from the Cigar Lake uranium deposit, Athabasca. *Earth Planet. Sci. Lett.* **2018**, *493*, 186–197.
17. Welhan, J.A.; Craig, H. Methane and hydrogen in East Pacific Rise hydrothermal fluids. *Geophys. Res. Lett.* **1979**, *6*, 829–831.
18. Neal, C.; Stanger, G. Hydrogen generation from mantle source rocks in Oman. *Earth Planet. Sci. Lett.* **1983**, *66*, 315–320.
19. Abrajano, T.A.; Sturchio, N.C.; Kennedy, B.M.; Lyon, G.L.; Muehlenbachs, K.; Bohlke, J.K. Geochemistry of reduced gas related to serpentinization of the Zambales ophiolite, Philippines. *Appl. Geochem.* **1990**, *5*, 625–630.
20. Sano, Y.A.; Urabe, T.; Wakita, H.; Wushiki, H. Origin of hydrogen–nitrogen gas seeps. *Oman. Applied Geochemistry*, **1993**, *8*, 1–8.
21. Charlou, J.L.; Donval, J.P.; Fouquet, Y.; Jean-Baptiste, P.; Holm, N.G. Geochemistry of high H_2 and CH_4 vent fluids issuing from ultramafic rocks at the Rainbow hydrothermal field (36°14′N, MAR). Chemical Geology **2002**, *191*, 345–359.
22. Guélard J.; Martinez I.; Sissmann O.; Bordmann V.; Fleury J.M. The role of ammonium in native H2 prodiction in continental lithosphere. In Proceedings of the Goldschmidt confonference, Boston, MA, USA August 2018; pp. 12–178, abstract.
23. Le Blancq, F. Diurnal pressure variation: the atmospheric tide. *Weather.* **2011**, *66*, 306–307. doi:10.1002/wea.857.
24. Carslaw, H.S and Jager, J.C. *Conduction of Heat in Solids*. Clarendon Press: Oxford, UK, 1959; pp. 510.
25. Luo, M.; Wood, J.R.; Cathles, L.M. Prediction of thermal conductivity in reservoir rocks using fabric theory. *J. Appl. Geophys.* **1994**, *32*, 321–334.
26. Baker, A.J.; Pepper, D.W. *Finite Elements 1-2-3*; McGraw Hill: New York City, NY, USA,1991, 341p.



© 2020 by the authors. Licensee MDPI, Basel, Switzerland. This article is an open access article distributed under the terms and conditions of the Creative Commons Attribution (CC BY) license (http://creativecommons.org/licenses/by/4.0/).